Chapter 4

A comprehensive investigation on afternoon transition of the atmospheric boundary layer over a tropical rural site

4.1. Introduction

The behavior of the ABL during the transition from a well-mixed layer during the day to a stably stratified layer during the night is quite complex and is also poorly understood. In recent years, the afternoon transition (AT) and evening transition (ET) of the ABL have gained attention for various reasons (*Lothon et al., 2014*). These transitional regimes are found to be important for the vertical transport of species, like pollutants, water vapor and ozone (*Klein et al., 2014*), the inception and strength of the nocturnal LLJ (*Mahrt, 1981; Van De Wiel et al., 2010*), and the whole structure of the nocturnal boundary layer. Furthermore, identification of the ABL becomes uncertain and there is no consensus on which scaling laws (day-time convective scaling due to surface buoyancy flux or nocturnal boundary layer scaling due to surface wind stress) would work well during this period (*Pino et al., 2006*). Furthermore, the start time of the transition and its duration could be different at the surface and aloft, because the turbulence may not immediately dissipate after the sunset (*Busse and Knupp, 2012*).

Researchers defined the transition in a variety of ways employing various parameters obtained from different instruments. Some of them treated the transition as an instantaneous process, while the others considered it as a process of a few hours. The most popular and widely used definition is the reversal of surface heat flux (positive to negative) (*Grant, 1997; Acevedo and Fitzjarrald, 2001; Beare et al., 2006; Angevine, 2008*). A similar technique is employed by *Nieuwstadt and Brost (1986)*, in which the AT is assumed to occur following the cessation of upward surface sensible heat flux. *Edwards et al. (2006)* noted that the shortwave heating starts to decrease long before the surface heat flux changes its sign. They included the shortwave heating in the definition of the AT, which shifted the start of afternoon transition to an earlier time. *Acevedo and Fitzjarrald (2001)* identified the start time of the transition from a sharp decrease in the spatial temperature difference and end from the maximum spatial standard deviation of temperature. As seen above, all these definitions are based on surface measurements and do not account for the physical processes occurring aloft during the transition.

The studies that used remote sensing measurements like wind profiling radars, sodars and lidars focused more on the processes aloft (mostly in the lower part of ABL) to define the AT. In a seminal study, *Mahrt (1981)* used a kinematic definition for the AT period. According to *Mahrt (1981)* the AT is a 4-5 h time period, starts from the time of low-level wind deceleration (typically 2 h before the sunset) and ends when the flow at all levels turned towards the high

pressure. *Grimsdell and Angevine (2002)* and *Angevine (2008)*, using radar wind profiler measurements, noticed that both reflectivity (range-corrected signal-to-noise-ratio (SNR)) and the spectral width (σ) (a measure of turbulence) decrease sharply during the AT. The applicability of these approaches is always an issue, particularly when the turbulence is either weak or strong throughout the day or when the turbulence increases due to some other processes associated with katabatic winds or land sea-breeze circulations (*Sastre et al., 2012*). Instead of defining the start and end times for AT, *Busse and Knupp (2012)* studied the variations in meteorological parameters with reference to the sunset time. They noted an increase in wind speed and a decrease in sodar return power in the lower ABL. They found that the AT has a relatively consistent pattern regardless of season. Recent times, *Wingo and Knupp (2015)* studied the variations in fluctating components of wind and temperature computed from nearly collocated surface, Doppler wind profiler, and vertically pointing Doppler lidar measurements. They show a consistent decline as turbulence intensity diminishes through transition.

A few studies employed models to understand or validate the occurrence of different types of transition (*Brazel et al., 2005; Edwards et al., 2006; Pino et al., 2006; Sorbjan, 2007; Nadeau et al., 2011; Sastre et al., 2012*). *Brazel et al. (2005)* studied the evening transition under weak synoptic forcing that favors the local thermal circulations and compared the observed transitions with models. Recently, *Sastre et al. (2012)* identified 3 types of evening transitions and evaluated performance of the Weather Research and Forecasting model (WRF) - Advanced Research WRF (ARW) model in reproducing these transitions by varying PBL parameterization schemes. They noted that all parameterizations reproduced the observed behavior of AT in certain circumstances. Noting the need to understand the transitions in a better way, several field campaigns were conducted in recent years, employing both in situ and remote sensors, exclusively for better characterization and modelling of the transitions, for instance, the CASES-99 (*Poulos et al., 2002*), BLLAST (http://bllast.sedoo.fr/) (*Lothon et al., 2014*) and TRANSFLEX (*Fernando et al., 2013*). Recently manned and unmanned aerial vehicles were used to study the vertical structure of the lowest part of the ABL during the AT (*Bonin et al., 2013; Lothon et al., 2014*). Furthermore, *Sastre et al. (2015)* performed a statistical analysis of AT between two different regions. According to them, at the drier region start time of AT occurs first than wet region.

Most of the above studies focused on the variations in state variables, like temperature, humidity, wind and turbulence, in the surface layer, as they are easily accessible. Other studies characterized the evening transitions aloft, but neglected the variations at the surface. Only a few studies that were based on campaign data and/or a few months of data dealt with the transitions in totality, i.e., studied the variations at the surface and aloft (*Busse and Knupp, 2012; Fernando et al., 2013; Lothon et al., 2014; Wingo and Knupp, 2015; Sastre et al., 2015*). Again, the data employed in those studies were limited: a few days to 2 months. Certainly there is a need to characterize and understand the transitions at the surface and aloft in different seasons through systematic observations on a long-term basis. Further, earlier studies used different state variables to define the transition. Only a few studies focused on how these state variables vary with reference to the time of sunset (*Busse and Knupp, 2012*). Although some tower-based observations exist in the literature, the complete understanding of the transition over a deeper layer is certainly far from complete. This forms the basis for the present study. In particular, the study tries to answer the following questions: how do the surface state variables and radar/sodar attributes vary during the transition and with reference to the time of sunset? Which state variable better identifies the transition? How does the start time of transition vary with height and season? Which physical processes are responsible for the vertical evolution of the transition?

This chapter is organized as follows: Section 4.2 introduces the data and instrumentation employed. The variation of different state variables at the surface and aloft is studied with the help of a typical case study in section 4.3. The start time of AT as identified by different state variables and their mean characteristics at the surface and aloft are studied with reference to the time of sunset. The questions posed above are discussed in light of present observations in section 4.4. The important forcing terms on the ABL are also estimated using a unique data set to understand the role of entrainment in the afternoon transitions. The important results are concluded in section 4.5.

4.2. Data and instrumentation

The present study relies on a variety of instruments, both in situ and remote sensors whose measurements cover the entire ABL. Two kinds of data sets (hereafter it is referred as data set 1 and data set 2) are used in the present study, but for different purposes. Data set 1 was collected with a suite of non-continuously operated instruments, spanning a 3-year period. This

data set is being used to examine the seasonality and height dependence of AT. It includes long-term observations made by an instrumented 15 m MBLM tower, a Doppler sodar and three UHF wind profilers (operated at NARL, but during different years) (see Table 4.1). Data set 2 is comprised of the intense observations, which include the instrumentation of data set 1 along with a flux tower having a sonic anemometer (RM Young 8100) at 8 m level and sondes (Meisei 90) launched every 3 h. Data set 2 was collected over two 3-day campaigns (one during the monsoon and one during the winter). This data set is being used to understand the role of surface forcing and entrainment in triggering the AT.

Table 4.1: Experimental specification files of SODAR, LAWP, WPR_{16x16} and WPR_{8x8}.

Parameter	SODAR	LAWP	WPR_{16x16}	WPR_{8x8}
Pulse width	180 ms	1 μs (uncoded)	4 μs (coded)	1 μs (uncoded)
Interpulse period (μs)	9×10^6	40	50	65
Range resolution (m)	30	150	150	150
Minimum height (km)	0.03	0.3	0.9	0.3
Maximum height (km)	1.5	4.8	6	7.65
Coherent integrations	1	70	32	32
Incoherent integrations	1	100	20	20
FFT points	4096	128	1024	1024
Beam directions*	E16, Z, N16	E15, Z, N15	E15, W15, Z, N15, S15	E10N10, W10S10, Zx, W10N10, E10S10
Data period	2007-2010	1999-2000	2010-2011	2010

* E, W, Z, N and S denote east, west, zenith, north and south directions, respectively, and the number indicates the off-zenith angle.

A series of automated tests were performed on tower time series data to identify instrumentation problems, flux sampling problems, and physically plausible but unusual situations (*Burba, 2013*). Furthermore, clear-sky days are identified from shortwave radiation measurements made by a pyranometer (Kipp and Zonen CMP6) located near the MBLM. Omitting the days with large data gaps and rain/dense clouds, 423 days of surface data were available for further analysis from 3 years of MBLM measurements. The range-time plots of

spectral moments (SNR, vertical velocity (w and σ from sodar and the wind profiler are examined for the clear growth and decay of ABL and convection/precipitation contamination (*Grimsdell et al., 2002; Rao et al., 2008a*). Based on the above criteria, a total of 530 and 482 clear-sky days of sodar and profiler, respectively, were only selected (from data set 1) for further analysis. To examine whether the filtering of data for clear-sky days has caused any bias towards the dry season (winter and summer), the data are segregated on the basis of the season. Table 4.2 shows the number of days for which the measurements were available, the number of discarded days due to rain, dense cloud or bad data quality and the number of days considered for the present study as a function of the season. Though considerable data were filtered out in the rainy seasons (southwest and northeast monsoons), the number of available days is large enough to represent the season. Also, the number of days available in the rainy season is on the same order as that of other seasons, indicating that the filtering has not biased the results towards any season.

Table 4.2: Details of data set 1 grouped as a function of season, showing the total number of days for which data are available, number of discarded days due to cloudy sky/rain or data gaps and number of clear days finally used in the present study. Win, Sum, SWM and NEM stand for, respectively, winter, summer, southwest monsoon and northeast monsoon.

Season	15m Tower (2009-2011)				Sodar (2007-2010)				Profiler (1999-00, 2010-11)			
	Win	Sum	SWM	NEM	Win	Sum	SWM	NEM	Win	Sum	SWM	NEM
Total no.of days	177	276	366	276	236	368	488	368	237	368	488	368
Instrument not functioning	64	81	103	55	19	35	74	113	129	130	107	104
Discarded due to rain	25	55	158	130	105	152	282	189	41	101	227	140
Final clear days	88	140	105	91	102	181	132	66	67	137	154	124

Note that MBLM, sodar and wind profilers were operated during different years. Only 19 days of simultaneous clear-sky measurements (without large data gaps) from all the above sensors were available. Measurements from these 19 days are used to understand the behavior of AT at different altitudes. The total data (from different years, i.e., data set 1) are used to obtain robust statistics on the mean behavior of the AT.

4.3. Results

4.3.1. Typical evolution of AT from the surface to the top of the ABL

Figure 4.1 shows the diurnal variation of surface state variables (T, water vapor mixing ratio (r, WS, wind variance (σ^2_{ws}) and wind direction (WD)) and sodar and profiler attributes (range-corrected SNR (hereafter referred to simply as SNR), horizontal wind speed, σ, w and wind direction) on 11 May 2010, providing a comprehensive paradigm of the typical evolution of the transitional boundary layer at the surface and aloft (up to 3.6 km). The surface state variables (at 5 m level) exhibit larger variations during the transition period than during the rest of the night. During the AT, as the shortwave heating decreases, the temperature decreases monotonically (Figure 4.1a) in clear-sky conditions, if temperature advection is neutral. Another signature of this transition can be seen in short-term variability of surface parameters, highly variable during the noon (associated with thermals) to smaller fluctuations in the night. The weakening of thermals (both magnitude and their vertical extent) in the afternoon reduces the convective turbulence and σ^2_{ws} (Figure 4.1d). This reduction weakens the downward transport of momentum and low-level wind speed (Figure 4.1c) (*Mahrt, 1981; Acevedo and Fitzjarrald, 2001*). The surface winds also became less gusty during the transition. During the day, when the convective turbulence is active, the low-level moisture gets diluted because of the transport of moisture by turbulence. As the turbulence decreases during the transition, the low-level moisture

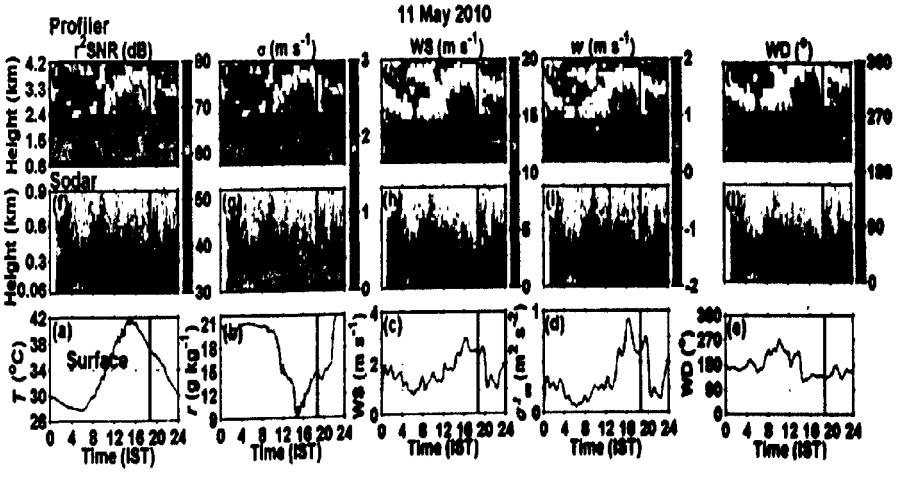

Figure 4.1: Diurnal variation of state variables at the surface and aloft on 11 May 2010, MBLM-derived surface (a) T, (b) r, (c) WS (d) σ^2_{ws} and (e) WD and sodar-derived (f) range-corrected SNR, (g) σ, (h) WS, (i) w and (j) WD. (k-o) Same as (f-j), except for profiler-derived state variables. The solid vertical line indicates the time of sunset.

having most of its sources on the Earth's surface increases in the absence of strong mixing (Figure 4.1b). On some days, this increase appears as a sudden jump, as also noted by earlier studies (*Busse and Knupp, 2012*), and on the other days it is more gradual. The wind direction nearly remains the same from ~14:00 IST (Indian Standard Time (IST) = UTC+05:30 h) to midnight (Figure 4.1e).

To understand the transitions aloft, variation of sodar and profiler attributes are examined in detail (Figure 4.1f–o). Figure 4.1 clearly shows the transition of the ABL from a highly convective to a more stable regime. When the convective turbulence is active during the day time, the thermals are clearly apparent as columns of enhanced backscatter in the time height SNR plot (Figure 4.1k). Though the thermals do not appear clearly in the SNR of sodar in this case, they appear very clearly in other cases. These plumes are also visible in the w plot (Figure 4.1i and n) as enhanced up- and down-ward motions with w values exceeding ± 2 m s^{-1} and as columns of enhanced turbulence (Figure 4.1g and l). The backscatter for sodar and profiler depends on the refractive index irregularities caused primarily by turbulence-driven temperature and humidity variations. The SNR is, therefore, high during the day, when the convectively driven turbulence is active. Nevertheless, about 2 h before the sunset, both the intensity and vertical extent of thermals start to decrease continuously till the sunset occurs. The minimum backscatter (SNR) is seen just before the sunset, mainly due to the weak turbulence. The magnitude of backscatter and vertical extent of sodar data again increase in accordance with the deepening of the inversion layer. As noted by *Busse and Knupp (2012)*, the winds within the nocturnal boundary layer generally decrease during the AT, but increase above the nocturnal boundary layer. It makes the identification of the start time of the AT using wind speed somewhat ambiguous. On the other hand, it is rather easy to identify the start time of the AT from the variations of SNR and σ. The wind direction does not change much with altitude below 1.5 km and remains mostly easterly to southeasterly (Figure 4.1j and o). It also does not change much with time around the time of sunset (a few hours before and after the time of sunset), ruling out the possibility of advection of different air masses causing the above changes.

When the surface heating reverses to cooling in the evening, both convection and turbulence gradually reduces till the subsequent development of a stable boundary layer with well-defined surface inversion layer. As a result, all state variables at the surface and aloft, manifested primarily by the turbulence, vary considerably during this period. To better depict

this variability, MBLM- (T, r, σ^2_{ws} and ΔT (T_5-T_{10} indicating the stability of the lower ABL; the suffixes 5 and 10 indicate the height of temperature measurements in m)), sodar- and profiler-derived state variables (SNR and σ at three representative levels; 150, 300 and 450 m for sodar and 900, 1500 and 2100 m for profiler) during the period 15:00 21:00 IST are plotted in Figure 4.2. To minimize random fluctuations and the chosen level more representative, the data are averaged both in time (5 min for sodar and no temporal integration for profiler) and height (three heights centred on the chosen level). The time series surface data are then low-pass filtered using local regression using weighted linear least squares and a first-order polynomial model (using the function "lowess" in matlab). On 11 May 2010, the temperature (Figure 4.2a) starts to decrease monotonically, at the rate of 1–1.5 °C per 1 h, from 16:10 IST (dashed line), 152 min prior to the

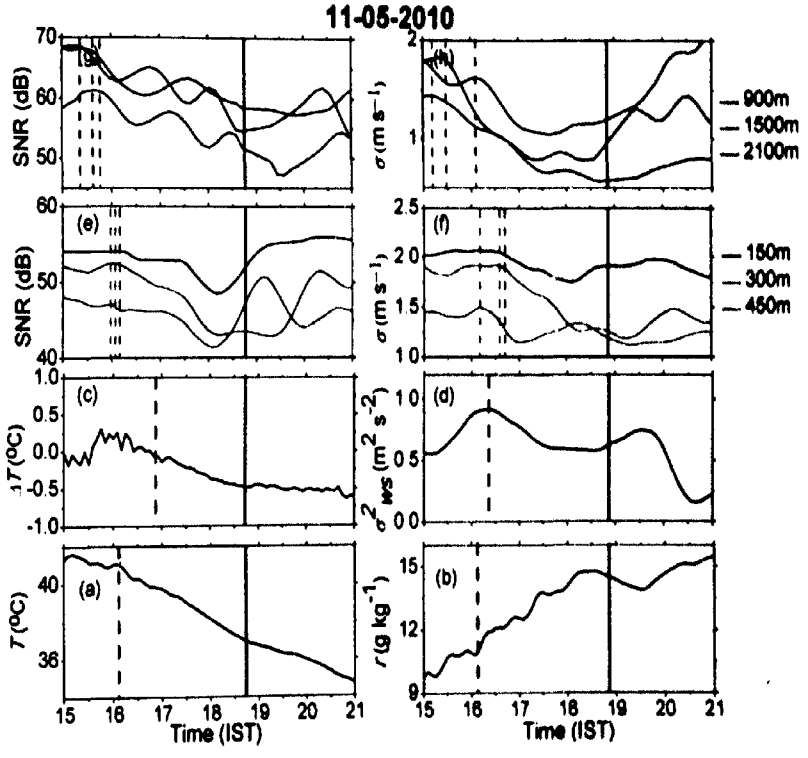

Figure 4.2: Temporal variation of state variables (at the surface and aloft) a few hours before and after the time of sunset (indicated with a black solid vertical line). Temporal variation of MBLM-derived (a) T, (b) r, (c) ΔT and (d) σ^2_{ws}, sodar-derived (e) range-corrected SNR and (f) σ and profiler-derived (g) range-corrected SNR and (h) σ. The sodar- and profiler-derived parameters are plotted at three representative levels each (150, 300 and 450 m for sodar and 900, 1500 and 2100 m for profiler). Vertical dashed lines indicate the start time of the transition as identified by different state variables.

time of sunset (solid vertical black line). Though the temperature decrement starts little early, but is not consistent and also weak in magnitude. Another surface characteristic showing a significant change during the AT is the mixing ratio (Figure 4.2b), which clearly shows a gradual increase from 16:10 IST. The temperature gradient (Figure 4.2c) also reverses from positive to negative few minutes after the 5 m level temperature starts to decrease. The wind variance (Figure 4.2d), representing small-scale wind fluctuations and turbulence, also shows a decreasing trend from 16:25 IST.

The sodar and profiler backscatter, depends primarily on turbulent irregularities of refractive index, decreases with the waning of sensible heat flux (and thermals) during the afternoon transition. On 11 May 2010, the SNR of sodar starts to decrease ~2 h 40 min prior to the time of sunset at all heights. Interestingly, the start time of SNR reduction shows height dependence with higher altitudes showing the reduction earlier. The SNR minimum is observed 10–20 min before the sunset at all heights, mainly due to the reduction in turbulent fluctuations in temperature. Nevertheless, the SNR increases again after the sunset, following the formation of an inversion layer. The σ (Figure 4.2f) variations are quite similar to that of SNR during the transition. The σ shows a decreasing trend 2 h 10–20 min prior to the sunset, whereas its minimum is observed 10–30 min from the time of sunset. The profiler SNR and σ variations are similar to that of sodar, except that their reduction starts little early. The profiler SNR and σ start to decrease ~3 h prior to the time of sunset. Also, the SNR and σ minima are observed at around the time of sunset. It is very interesting to note the height dependency in the time at which state variables show large variation; i.e., it is seen first in profiler attributes, then in sodar attributes and finally in surface parameters.

4.3.2. Distributions for start time of transition with reference to the time of sunset

It is clear from the case study that the surface parameters and sodar/profiler attributes show large variations during the AT. The first and foremost problem, therefore, is to properly and objectively identify the start time of AT from these state variable. It is also important to recognize the state variable that unambiguously identify the start time of transition. As seen in case studies, state variable like T, ΔT, r and σ^2_w at the surface and SNR and σ aloft can be used for this purpose. For identifying the start time of AT, the 19 days on which measurements of all instruments (MBLM, sodar and profiler) are available are considered. The start time of AT is

identified manually from temporal variation of each state variable (like those shown in Figure 4.2). The temporal gradients are estimated for each state variable from all 19 cases, which are then finally used to fix the thresholds. The start time of transition is identified from the variation of the each state variable as follows.

Temperature: the time at which T starts to decrease by ≥ 0.5 °C in 30 min.

Water vapor mixing ratio: the time at which r increases by ≥ 0.5 g kg^{-1} in 30 min.

Wind variance: the time at which σ^2_{ws} decreases by ≥ 0.1 m^2 s^{-2} in 30 min.

Temperature gradient: the time at which ΔT becomes positive to negative and remains negative for at least an hour.

SNR: the time at which SNR decreases by > 1 dB in 30 min.

Spectral width: the time at which the σ decreases by ≥ 0.1 m s^{-1} in 30 min.

Note that all the above conditions should hold good for at least an hour from the start time of the transition. Also, all the above conditions are checked only in the data during 15:00-20:00 IST.

First, the average behavior of the start time of the AT, as identified by selected state variables, with reference to the sunset (i.e., start time of the AT - time of sunset) has been studied at the surface and aloft. The distributions (from data set 1) for the start time of the AT with reference to the sunset (hereafter referred to as $\text{Trans}_{\text{sunset}}$ (start time of the AT - time of sunset)) as obtained by various state variables are shown in Figure 4.3. These distributions are shown as boxplots, where the box comprises 50% of values (25th and 75th percentiles) and whiskers represent 5th and 95th percentile values. On average, σ^2_{ws} and T show the first signature of the AT among all surface state variables (Figure 4.3a), ~1 h 40 min prior to the time of sunset, followed by ΔT (1 h 18 min before sunset). The last characteristic for the transition is seen in r as a gradual increase (or jump) occurring 1 h 10 min prior to the time of sunset. The signature of the transition can be seen as early (late) as 165 (45) min before (after) the sunset in σ^2_{ws} (r on some days. Except for temperature, all other surface state variables show the signature of the transition even after the sunset. Though not many such cases are found at Gadanki (can be seen from Figure 4.3a), late transitions are not uncommon, as they are widely reported elsewhere (*Acevedo and Fitzjarrald, 2001*). The distribution of $\text{Trans}_{\text{sunset}}$ is wider for r than for any other state variable, indicating that the jump in r occurs at different timings with reference to the time of

sunset. On the other hand, the start time of the AT as obtained by T is relatively consistent throughout the year, as evidenced by the narrow distribution (Figure 4.3a).

Figure 4.3b g shows distributions for $Trans_{sunset}$ as identified by selected sodar and profiler attributes (SNR and σ at three selected altitudes (150, 300 and 450 m for sodar and 900, 1500 and 2100 m for profiler). At any particular altitude, both SNR and σ show the signature of the transition around the same time. Though small differences exist, they are not significant. Nevertheless, the identification of the transition start time is somewhat easy with SNR and is also consistent, as evidenced by its relatively narrow distribution. As seen in the case study, the mean start time of the AT also shows height dependency and follows top-to-bottom evolution; i.e., the signature of the AT is seen first in the profiler data (~2 h 40 min before the time of sunset), then

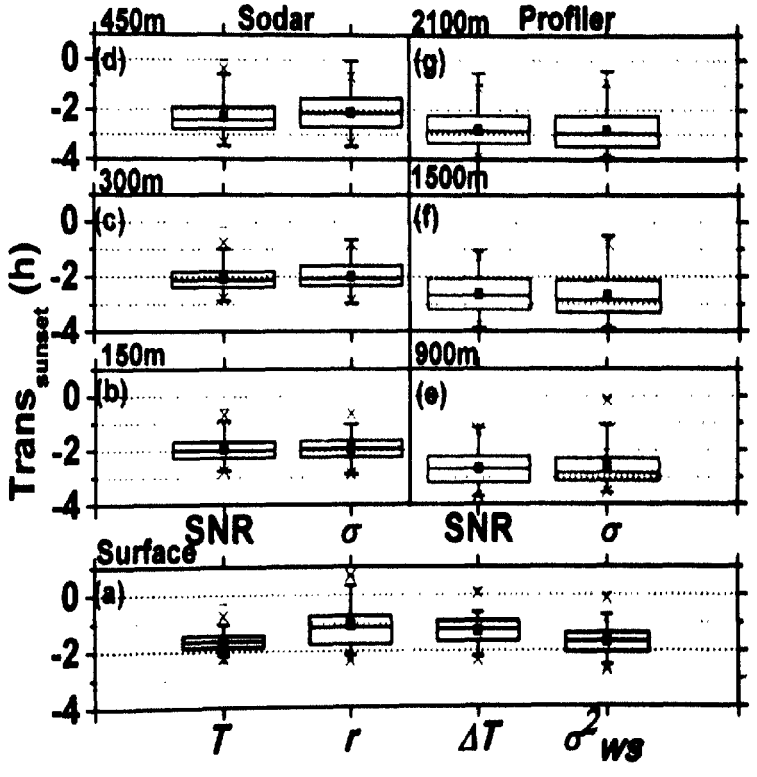

Figure 4.3: Distributions (in terms of boxplot) of $Trans_{sunset}$ (= start time of AT - time of sunset) for different state variables, depicting the behavior of the transition start time with reference to the sunset time. Distributions for $Trans_{sunset}$ at (a) the surface (obtained from T, r, ΔT and, σ^2_{ws} (b–d) 150, 300 and 450 m, respectively (obtained from sodar-derived range-corrected SNR and σ and (e–g) 900, 1500 and 2100 m, respectively (obtained from profiler-derived range-corrected SNR and σ.

in sodar data (~2 h before the time of sunset) and finally in MBLM measurements. *Angevine (2008)* also noted the deterioration of the ABL structure aloft with the wind profiler preceding the start time of the AT at the surface. It contradicts the general perception that the entire ABL is controlled primarily by the underlying Earth's surface and the start time of transition should follow a bottom-up evolution. It is true that surface forcing is the defining mechanism during the day, but it seems not the case during the transition, the time during which other forces could also be important.

A sensitivity analysis is carried out to know the impact of the above chosen thresholds on $Trans_{sunset}$ as obtained by different state variables. The chosen thresholds are varied by ±20% in steps of 10% and the mean $Trans_{sunset}$ as obtained by different state variables is estimated at different altitudes. The mean $Trans_{sunset}$ as a function of altitude is plotted in Figure 4.4, which clearly shows that the important results do not change much, even if the thresholds are varied by ±20%. For instance, the mean $Trans_{sunset}$ does not change much with the variation of thresholds. Also, the height dependence of $Trans_{sunset}$ is strikingly apparent with all used thresholds. It

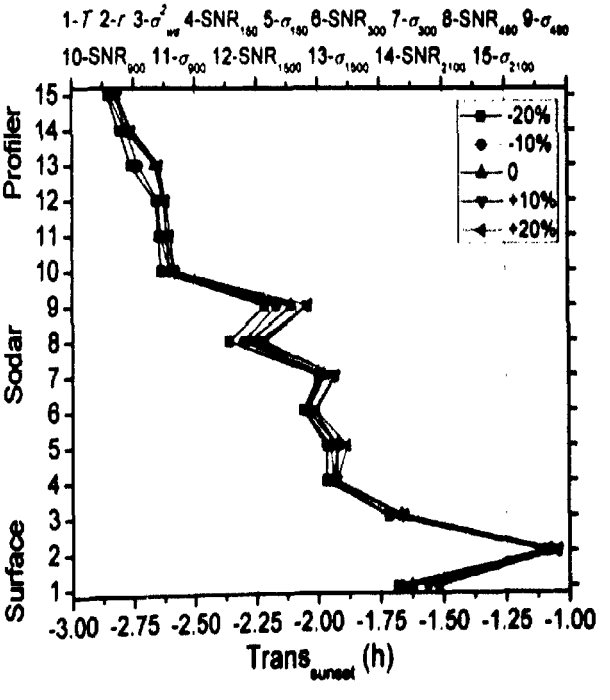

Figure 4.4: Variation of mean $Trans_{sunset}$ as obtained by different state variables for different thresholds, depicting the sensitivity of thresholds used in the present study to the start time of the transition.

suggests that the observed variability in $Trans_{sunset}$, like top-to-bottom evolution, is not an artefact arising due to the chosen thresholds. Regarding the usability of these thresholds at other sites, it appears (from Figure 4.4) that they possibly can be used at other tropical sites, which are in similar climatic conditions as Gadanki region. Although we expect similar variations in most of the state parameters at mid- and high latitudes, the magnitude of variation could be different because of the differences in the solar zenith angle and rate of reduction of solar radiation during the transition. Therefore, some tuning of thresholds may be required at different latitudes.

4.3.3. Seasonal variation in the start time of the transition

Gadanki experiences different seasonal patterns: very hot and dry summer, hot and rainy southwest monsoon, cool and rainy northeast monsoon and cool and dry winter. These seasonal factors (solar exposure, synoptic flow, soil condition, etc.) will have a different impact on the ABL, in general, and transitions, in particular. Therefore, the distributions of $Trans_{sunset}$ for different seasons (Figure 4.5) have been studied to understand the impact of the above factors on the start time of the transition. Figure 4.5a-d reveals that the order in which the surface state variables show the transition remain nearly the same (the monsoon season is an exception), but their occurrence time with reference to the sunset varies considerably. Although reduced compared to the total data (Figure 4.3), the distribution, representing the variability within the season, of the transition start time for each state variable is quite wide. The $Trans_{sunset}$ distribution for T shows a consistent pattern regardless of the season, with small variability within the season, and the transition starts 80–100 min prior to the time of sunset. Nevertheless, it exhibits a clear seasonal variation with dry seasons (winter and summer) showing the transition early (~110 min prior to the sunset time) compared to rainy seasons (80 min prior to the sunset time). The distributions for other state variables also show some seasonal variation, with warm seasons showing the transition a little earlier than cold seasons. But, their distributions are much wider than the observed weak seasonal variation. Among all state variables, the $Trans_{sunset}$ distribution for r shows not only large seasonal variability, but also a wide distribution, indicating the highly variable nature of the r jump (i.e., starts at different timings with reference to the sunset).

Two representative heights, 300 m from the sodar and 1500 m from the wind profiler, are chosen to study the seasonal variation in the transition start time aloft (Figure 4.5e-l). Like in Figure 4.3, there is not much difference in the start time of transition by SNR and σ in any season

and at any particular altitude. Two observations are strikingly apparent from Figure 4.5. 1. Both profiler- and sodar-derived start times of transition show some seasonal variation with delayed transition during the northeast monsoon, consistent with the seasonal variation at the surface. 2. Irrespective of the season, the height dependency in the transition start time is intact. Both these issues are discussed in detail in section 4.4.

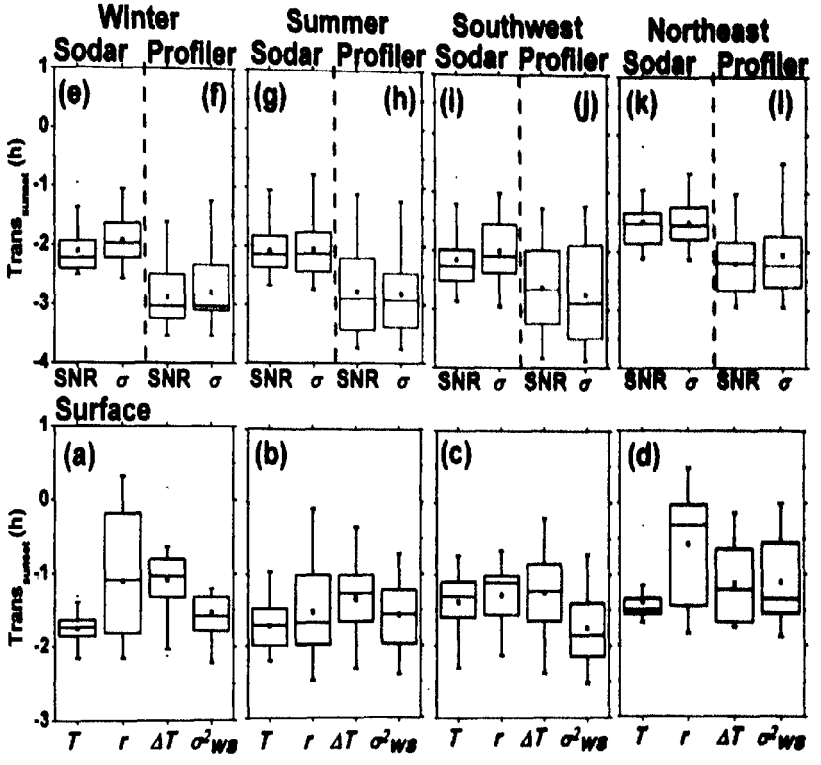

Figure 4.5: The distributions of $Trans_{sunset}$ as obtained by different surface state variables for (a) winter (b) summer (c) southwest monsoon and (d) northeast monsoon, depicting the seasonal variability in the start time of the transition. The distributions for $Trans_{sunset}$ as obtained by sodar-derived range-corrected SNR and σ at 300m for (e) winter, (g) summer, (i) southwest monsoon and (k) northeast monsoon, respectively. (f), (h), (j) and (l) are the same as (e), (g), (i) and (k), except for profiler-derived range-corrected SNR and σ at 1500 m.

4.4. Discussion

The four major questions related to the start time of transition that the paper tries to answer are (i) which state variable better identifies it, (ii) does it exhibit any seasonal variation, (iii) does it show any height dependency, and (iv) which physical mechanism is responsible for the observed height variation of $Trans_{sunset}$?

i. Among all state variables, the decrease in temperature at the surface and SNR aloft are strikingly apparent in all case studies, which makes them ideal for identifying the start time of the AT. Furthermore, the distributions of $Trans_{sunset}$ for T and SNR are somewhat consistent and narrower than that for other state variables. Although several earlier studies employed reversal of sign in surface heat flux as a criterion for transition (*Lothon et al., 2014*, and references therein), it is now well known that such a reversal does not always occur during the transition (*Busse and Knupp, 2012*). The formation of an inversion depends on several other factors and therefore the formation of inversion alone cannot be used to define the transition. A few studies used deceleration of low-level wind as a criterion for identifying the transition (*Mahrt, 1981*). The above criterion works well in the lower portion of ABL, but fails above the nocturnal boundary layer, where the wind accelerates in the frictionless fluid. Therefore, T at the surface and SNR aloft can be used to identify the start time of the transition, as also suggested by *Edwards et al. (2006)*.

ii. The start time of the transition as defined by different state variables shows some seasonal variation, with late transitions during the northeast monsoon season. Though Gadanki receives 55% of the annual rainfall in the southwest monsoon, raising instantaneous soil moisture levels, the high insolation and temperatures immediately consume the soil moisture for latent heating. On the other hand; this region also gets a good amount of rainfall during the cool northeast monsoon (*Rao et al., 2009b*). The soil moisture levels, therefore, remain high in this season. It is known from earlier studies that the abundance of soil moisture not only produces shallow ABL, but also delays the growth of the ABL (see Figures 3.12c and 3.13c). It appears from present observations that not only the growth but also the descent (or transition) is getting delayed due to the excess soil moisture.

iii. The total and seasonal distributions of $Trans_{sunset}$ for different state variables at the surface and aloft clearly show the height dependency in the start time of transition, following a top-to-bottom evolution. It is known from the literature that there exists an apparent contradiction between those who think the transition starts in the afternoon at high levels (*Angevine, 2008*) and others who believe the AT occurs around the sunset and follows a bottom-up evolution. The present study supports the former view, as similar evolution is seen in total and seasonal plots (Figures 4.3 and 4.5). During the AT, when the surface buoyancy flux decreases toward zero, the influence of other competing processes like advection, and entrainment becomes

relatively more important (*Bosveld et al., 2014*). Therefore an attempt has been made to estimate these fluxes (buoyancy and entrainment) to understand their roles in the observed height dependency in transition start time.

The ratio between the vertical kinematic eddy heat flux at the top of ABL and kinematic eddy heat flux at the surface (*Sun and Wang, 2008*) (entrainment ratio), as given below, therefore, becomes a fundamental and decisive parameter.

$$A_r = -\frac{\overline{(w'\theta')}_{zi}}{\overline{(w'\theta')}_s} \qquad (4.1)$$

The heat flux at the top of ABL (or entrainment flux) is estimated following *Angevine (1999)*. The entrainment can occur due to any or all of these factors: (1) when there is a shift in the ABL height (2) due to wind shear at the surface, (3) due to wind shear at the top of the ABL and (4) advection.

$$-\overline{(w'\theta')}_s = A_0 + (A_2 u_*^2 \bar{u} + A_3 \Delta u_h^3).\frac{\theta_{v0}}{g d_1} + (U\frac{\partial T}{\partial x} + V\frac{\partial T}{\partial y}) \qquad (4.2)$$

where u_* is the friction velocity, $\bar{u}$ the surface horizontal velocity (8 m in our case), Δu_h the wind shear at the top of ABL, g the acceleration due to gravity, θ_{v0} the virtual potential temperature at the surface, $d1$ is the depth of entrainment zone and A_2 and A_3 are empirical constants, $A_2 = 0.005$ and $A_3 = 0.01$ (*Stull, 1976*). For the estimation of advection (last term in Eq. 4.2), the temperature (T, horizontal distance in zonal and meridional planes (∂x and ∂y, respectively, and is equal to 0.5°) and zonal (U) and meridional (V) wind velocities near the top of ABL are taken from ECMWF Interim Reanalysis data (*Dee et al., 2011*). A_0 is the entrainment flux in the absence of any mechanical term contribution and is expressed as $w_e\Delta\theta$. w_e is the entrainment velocity and is estimated as follows.

$$w_e = \frac{dz_i}{dt} - \bar{w} \qquad (4.3)$$

where $\bar{w}$ is the average vertical velocity at the top of ABL and $\Delta\theta$ the vertical gradient in θ_v at the top of ABL. As seen above, the timescales and space scales of different entrainment processes cover a wide range, which makes it difficult to measure or model accurately (*Angevine, 1999*). Although it is possible to quantify the entrainment flux from the heat budget equation (Eq. 4.2), the uncertainties in the basic parameters (for instance, those in the advection

term and w hamper the accuracy of the flux. Therefore, as also pointed out by *Angevine (1999)*, these numbers need to be considered as the "best available estimates".

It is clear from the above equations that profiles of meteorological parameters such as T, RH/r and w are essential to estimate the entrainment ratio. Though w can be obtained continuously from the wind profiler, continuous measurement of T and RH/r at the top of the ABL is a difficult task. We, therefore, considered two 3-day campaign data (one each from the southwest monsoon and winter), wherein sonde ascents were made once in ~3 h, for a detailed study (data set 2).

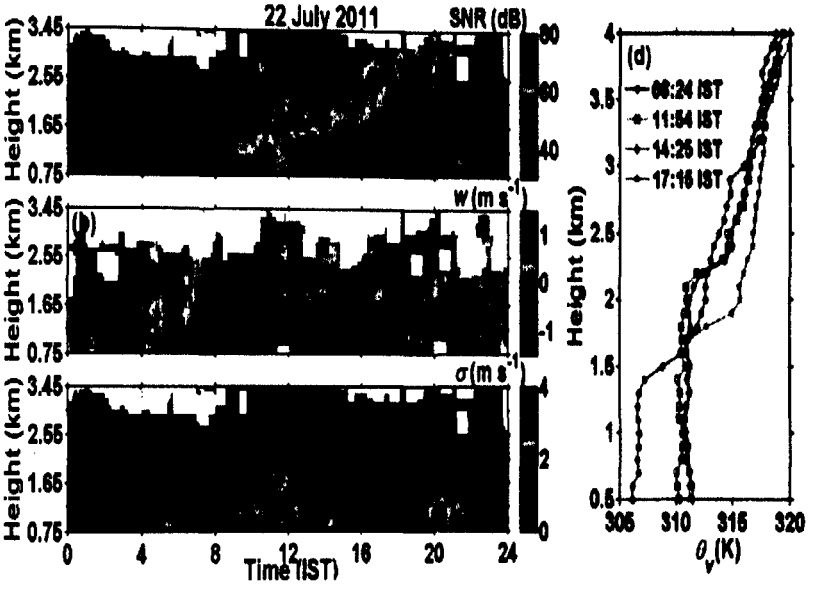

Figure 4.6: Diurnal variation of profiler attributes (a) range-corrected SNR (b) w and (c) σ on 22 July 2011, illustrating the evolution of the ABL and afternoon transition. (d) The vertical variation of radiosonde-derived Θ_v at ~ 3 h intervals. The solid symbols in (a) indicate the height of the ABL.

Figure 4.6a–c shows the time–height variation of SNR, w and σ on 22 July 2011, depicting the typical diurnal evolution of the ABL during the campaign period. The Θ_v profiles during the morning-evening (at 08:24, 11:54, 14:25 and 17:15 IST) period are shown in Figure 4.6d to depict the height of the ABL (and also the gradients in Θ_v at the top of the ABL). Clearly, the height of the ABL as obtained by the profiler (shown with dots on the SNR plot) and sonde (the gradient in Θ_v profile) corresponds well. The agreement between them is also good in the diurnal variation, with both the measurements showing a shallow ABL in the morning and evening transition periods and a deep ABL during the day, when the ABL is convectively active.

The start time of AT as seen by different state variables at the surface and aloft on all days during the two campaigns is shown in Figure 4.7a and b. It clearly reiterates the height dependency of the start time of AT seen in Figures 4.2 4.5; i.e., the start time of AT observed by the profiler precedes surface state variables on all days and in both seasons. Though the same pattern is seen on all days, the time at which the transition starts varies considerably from day to day. The entrainment flux at the top of ABL is estimated by combining the measurements of sonde ($\Delta\theta$, dl), profiler (w, Δu_h), MBLM (u, θ_w) and a meteorological flux tower (u_*) with ECMWF interim data (advection term). The sensible heat flux and u_* at the surface required to quantify the entrainment ratio (Eq. 4.1) are estimated following the eddy covariance method by using 20 Hz resolution ultrasonic anemometer measurements at 8m level. These fluxes are evaluated at 30 min resolution.

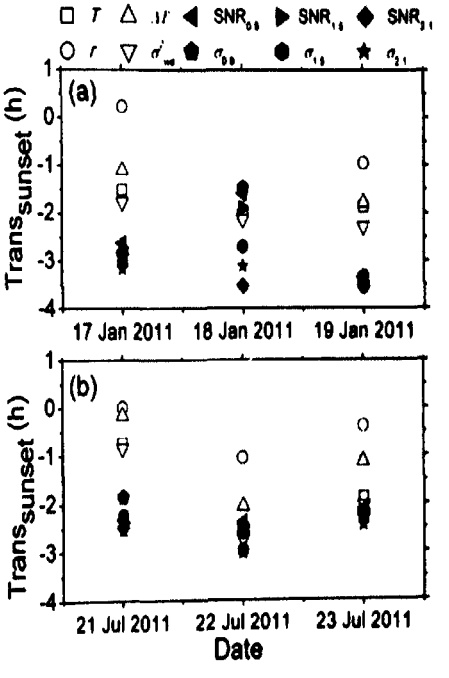

Figure 4.7: The start time of the AT with reference to the time of sunset as obtained by different state variables at the surface and aloft during (a) 17–19 January 2011 and (b) 21–23 July 2011.

Figure 4.8a and b shows the sensible and entrainment fluxes at ~ 3 h resolution during the day, depicting the forcing on the ABL from bottom and top. The sensible heat flux varies considerably during the day, with fluxes varying from 0.15 0.25 K m s^{-1} around noon (~11:00

and ~14:00 IST) to 0.02–0.07 K m s^{-1} during the morning and evening transitions (~08:00 and ~17:00 IST). On the other hand, the entrainment flux neither changes drastically during the day nor shows a clear diurnal cycle (compared to sensible heat flux). The magnitude of entrainment flux depends mostly on the first term in Eq. 4.2, while the shear (2 and 3 terms in Eq. 4.2) contributes very little to the total entrainment flux (not shown). Since the buoyancy flux changes considerably, the entrainment ratio varies significantly during the course of the day. The entrainment ratio increases to 0.5–1.1 during the morning and evening transitions. Therefore, it is very clear from these observations that the forcing from the top (i.e., entrainment flux) becomes very important, when the buoyancy flux is weak (i.e., during the transitions and night). A few earlier studies also underscored the importance of buoyancy flux in altering the structure of the ABL. The entrainment not only modifies the top of the ABL but also impacts the entire depth of the ABL (*Lohou et al., 2010*). *Caughey and Kaimal (1977)*, have shown experimentally that the heat flux descents suddenly during the transition, approximately an hour before the sunset, and the reversal of heat flux (from positive to negative) first occurs at higher altitudes and then propagates downwards to the surface, indicating the importance of entrainment heat flux in the top-to-bottom evolution of the transition.

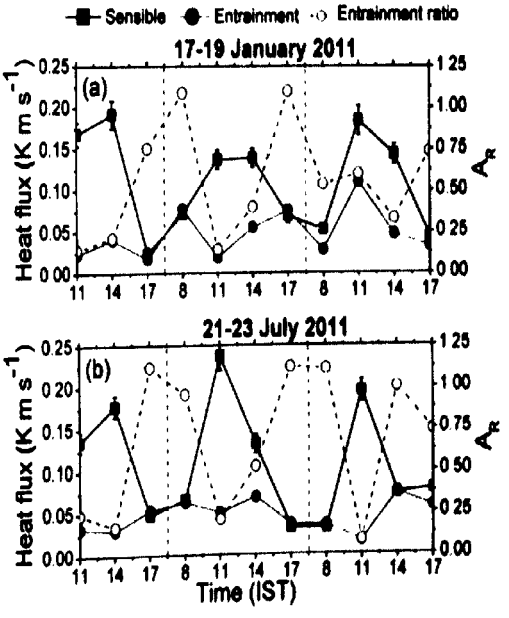

Figure 4.8: Sensible and entrainment fluxes (left axis) and entrainment ratio (right axis) estimated at ~ 3 h intervals during (a) 17 19 January 2011 and (b) 21 23 July 2011, indicating the forcings on the ABL from the bottom and top.

Also, with continuous waning of sensible heat flux during the AT, both the vertical extent and strength of thermals (can be seen in Figures 4.1 and 4.6) decrease monotonously. At the same time, the surface forcing (heating) remains good enough to maintain the turbulence close to the surface and therefore does not show the signature of transition, but delays it at the surface (*Angevine, 2008*).

4.5. Conclusions

This study presents a comprehensive view of the AT in terms of understanding the variability of different state variables using a suite of in situ and remote sensing measurements at Gadanki. The study aims to address the following issues related to the start time of AT with a unique and statistically robust data set (~3 years). Which parameter first shows the signature of transition at the surface and aloft? Which parameter better defines or identifies it? How does it vary with altitude and season? Which physical mechanism explains the observed vertical variation of transition?

1. Among the surface state variables, the signature of transition is first seen in σ^2_{ws} and T data, both of which start decreasing monotonically ~100 min prior to the time of sunset. The r increase is the last signature of transition, while the reversal of ΔT variation from positive to negative falls in between these extremes. Aloft, both SNR and σ identify the start of the AT at the same time, 120–160 min prior to the time of sunset, depending on the height considered. The observed mean start time of the AT (2 h prior to the sunset), obtained from SNR and σ variations, matches well with that obtained by *Mahrt (1981)*, who used horizontal wind reduction for identifying the transition.

2. At the surface, the start time of AT can be discerned more easily from variations of T than from that of σ^2_{ws}, r and ΔT. While σ^2_{ws} and ΔT variations show large modulations with time, r variation is ambiguous at times. Also, the temperature reduction is more consistent with relatively narrow distribution and occurs always before the sunset. Aloft, SNR variation is robust in identifying the transition compared to ambiguous variations in horizontal wind velocity (decreases at lower altitudes and increases at higher altitudes).

3. The start time of the AT as defined by different state variables shows some seasonal variation, with delayed transitions during the northeast monsoon at the surface and aloft. Though there

is some seasonal variation in the start time of the AT relative to sunset time, the order in which the signature of the AT is seen in different state variables (first in T, and σ^2_{ws} followed by ΔT and r remained nearly the same in all seasons.

4. Interestingly, the start time of the AT exhibits a clear height dependency; i.e., the signature of the transition is seen first in profiler attributes (~160 min) followed by sodar attributes (~120 min) and finally in surface state variables (~100 min), suggesting that the transition follows a top-to-bottom evolution (*Angevine, 2008*). The fact that the first signatures of the transition are seen at higher altitudes by profiler/sodars than at the surface suggests that forces other than the buoyancy could also play an important role during the transition. With continuous waning of sensible heat flux (and surface forcing) during the AT, both the vertical extent and the strength of thermals decrease steadily (as seen in Figures 4.1 and 4.6), triggering the descent of the ABL or the transition. However, the surface heating is good enough to maintain the state variables and delay the decrease in T and σ^2_{ws} (considered to be the signatures of the transition). Furthermore, the impact of forcings from the top and bottom on the ABL is studied by quantifying the sensible and entrainment fluxes, using a flux tower and profiler-sonde measurements, respectively. Though the sensible heat flux varied significantly during the day, the entrainment flux remained nearly the same throughout the day. The entrainment ratio increases considerably during the morning and evening transitional periods, primarily due to the weak sensible heat flux. Therefore, the entrainment flux appears to be playing a major role during the transition period (and in the night) during which the sensible heat flux continuously weakens.